

Article

Analysis on Electromagnetic Field of Continuous Casting Mold Including a New Integral Method for Calculating Electromagnetic Torque

Shaoliang Li ¹, Hong Xiao ^{1,2}, Pu Wang ¹, Huasong Liu ¹ and Jiaquan Zhang ^{1,*}

¹ School of Metallurgical and Ecological Engineering, University of Science and Technology Beijing, Beijing 100083, China

² Electromagnetic Center, Hunan Zhongke Electric Co., Ltd., Yueyang 414000, China

* Correspondence: jqzhang@metall.ustb.edu.cn; Tel.: +86-010-6233-4222

Received: 24 July 2019; Accepted: 27 August 2019; Published: 29 August 2019



Abstract: Based on the Maxwell's equations, a finite element model is established to study the characteristics of electromagnetic field in the mold of billet and bloom continuous casting with electromagnetic stirring (M-EMS). A novel integral method for calculating electromagnetic torque is proposed to evaluate the stirring intensity of stirrer. In order to verify the accuracy of the model, a well-designed electromagnetic torque detecting device is fabricated. The predicted value of electromagnetic torque and magnetic flux density are consistent with the measured data. The optimum frequency is determined by the maximal electromagnetic torque of the strand. The effect of stirring current intensity and different stirrer positions along the length of mold on the electromagnetic field has been studied numerically. The results show that the optimum frequency is smaller when the copper tube of the mold is thicker and the section size is bigger. Besides, the electromagnetic torque of the strand is a quadratic function of the running current intensity. Moreover, the installation position of stirrer strongly affects the prediction of electromagnetic field distribution, further influencing the optimum frequency and the electromagnetic torque of strand.

Keywords: mold electromagnetic stirring; electromagnetic field; electromagnetic torque; optimum frequency; installation position; numerical simulation

1. Introduction

Mold electromagnetic stirring (M-EMS) is widely used in the billet and bloom continuous casting process for improving the as-cast quality effectively. Generally, an alternating magnetic field with low frequency is adopted by the stirrer. When an alternating magnetic field is applied to a conductor, it induces eddy current in the conductor. The interaction between the alternating field and eddy current generates an electromagnetic force, which is known as Lorentz force. In consequence, the function of M-EMS is to produce Lorentz force in the conductive molten steel, which forces the liquid steel into swirling flow. By altering the fluid flow in the mold, the M-EMS is meant to improve the heat transfer at the solidification front, accelerate the superheat dissipation of melt [1,2], and promote the transition from columnar to equiaxed crystal during solidification subsequently [3–5]. Besides, the surface defects and sub-surface cleanness can be well controlled by a favorable flow pattern in the continuous casting mold [6–8].

Magnetic flux density is an important parameter of the electromagnetic field, which can be offline (without strand), measured by a gauss meter directly in the plant. The measured magnetic flux density can be used to verify the actual working condition of the stirrer. However, the magnetic flux density is an intermediate parameter between the excitation current and the induced electromagnetic force in the

melt, which can not reflect the stirring intensity of the stirrer directly. The induced electromagnetic torque is in-fact the motivation of driving the molten steel into swirling flow. Thus, the electromagnetic torque is a more appropriate evaluating index of the stirring intensity than the magnetic flux density. However, the measurement of the electromagnetic torque of melt in the mold is difficult. An et al. [9] tried to measure the electromagnetic torque using aluminum alloy probes, but he didn't present the computing method. Beitelman [10] gave the analytical expression of the electromagnetic torque as:

$$T = 0.25\pi\sigma\omega B^2 R^4 L, \quad (1)$$

However, the value of magnetic flux density B in the melt changes with different positions. So, the analytical value T only represents the electromagnetic torque at a specific location, which can not reflect the electromagnetic torque of the whole strand accurately. The calculation method for the electromagnetic torque of the entire conductor in the harmonic electromagnetic field still remains unclear.

As we know, the continuous casting machine is a highly integrated mechanical apparatus with a variety of auxiliary equipment, and each component has a fixed position for working effectively. However, the placement of the M-EMS is still controversial. It is desirable to put the stirrer at such a location to provide an ideal stirring intensity distribution between the meniscus zone and the bulk of the mold. The confined space available for the stirrer is a major factor affecting the installation location. Some are installed in a lower part of the mold to minimize the stirring action in the meniscus region [11–13], and some are positioned at the middle area of the mold due to the limited space constraint of the casting machine [2,14]. Unlike the final electromagnetic stirring (F-EMS), there is a copper-alloy mold between the stirrer and the molten steel for M-EMS. The electromagnetic field is severely weakened in the presence of a copper mold with good conductivity due to the electromagnetic shielding effect. Thus, the electromagnetic field is strongly affected by different relative positions of the stirrer and mold. However, the effect of stirrer installation position on the electromagnetic field distribution has been rarely researched.

In this study, a novel integral method based on the finite element model is proposed to calculate the electromagnetic torque of the whole strand in the computational domain. A well-designed electromagnetic torque detecting device was fabricated, and the numerical model was verified by measurement. The characteristics of the electromagnetic field were analyzed numerically. The optimum frequency was confirmed by the maximal electromagnetic torque of the strand. The influences of stirring current intensity and different stirrer installation positions on the electromagnetic field were investigated in detail.

2. Mathematical Model

The schematic diagram of the billet continuous casting mold with electromagnetic stirring discussed in this study is presented in Figure 1. The structure of iron core with six coils around the salient iron poles is applied to the stirrer. The excitation source of the stirrer is three-phase alternating current power, which generates a harmonic electromagnetic field. The model of M-EMS mainly includes iron core, stirring coil, copper mold, molten steel or measuring probe, and air (not shown). The volume of the air domain is ten times that of the stirrer to capture the majority of the electromagnetic field.

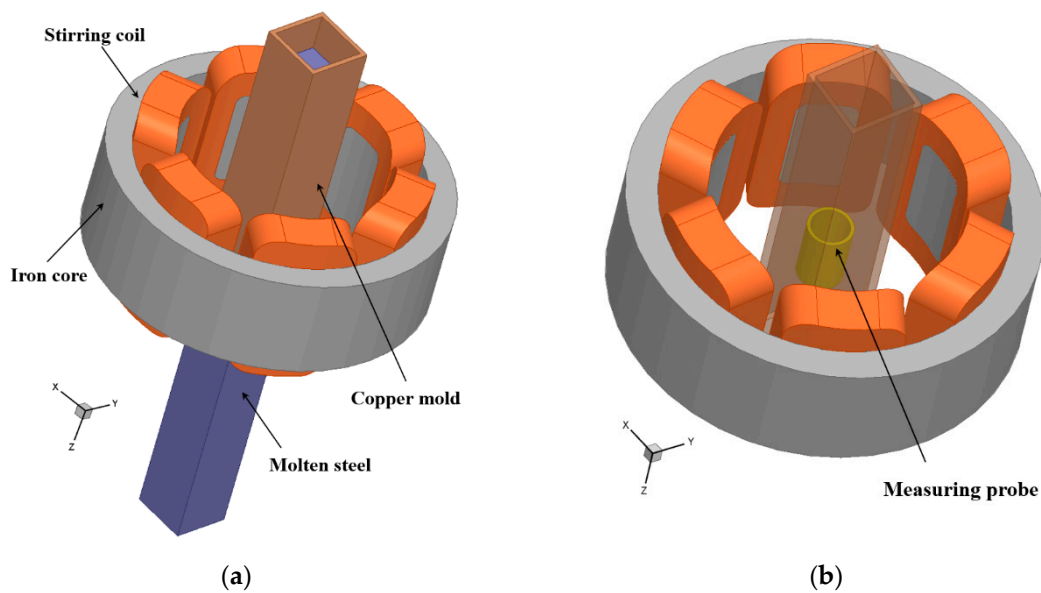


Figure 1. Schematic diagram of the model: (a) with strand; (b) with probe.

2.1. Assumptions and Simplified Mathematic Model

1. The induced magnetic field in the melt is ignored by comparison with the imposed magnetic field B [15].
2. For the continuous casting process with M-EMS, the magnetic Reynolds number $R_m \ll 1$, so the effect of the melt flow on the electromagnetic field is negligible. In consequence, for Ohm's Law $J = \sigma(E + u \times B)$, the term of $(u \times B)$ is neglected [16].
3. The electromagnetic field phenomena of the M-EMS is supposed to be a magneto quasi-static problem due to the low frequency. The displacement current $\partial D / \partial t$ in Maxwell's equations is neglected.
4. The cooling water of the mold and the insulation materials of the stirrer are considered to be air in the model, since their relative permeability is close to 1.
5. The iron core of stirrer is supposed to be isotropic with a constant permeability.

2.2. Governing Equations

At the low frequency of the mold electromagnetic stirring, the description of the Maxwell's equations of electromagnetic field is as follows. The Gauss's law in Maxwell's equations is not presented because it is not used in the model.

Gauss's law for magnetism:

$$\nabla \times B = 0, \quad (2)$$

Ampere's law:

$$J = \nabla \times \frac{B}{\mu}, \quad (3)$$

Faraday's law:

$$\nabla \times E = -\frac{\partial B}{\partial t}, \quad (4)$$

Ohm's law:

$$J = \sigma E, \quad (5)$$

where B is the magnetic flux density, T; J is the induced current density, $A \cdot m^{-2}$; E is the electric field strength, $V \cdot m^{-1}$; μ is the magnetic permeability, $H \cdot m^{-1}$; σ is the electrical conductivity, $S \cdot m^{-1}$.

The exciting current is sinusoidal for the M-EMS, so the electromagnetic field is harmonic. The magnetic flux density and induced current density are complex number form, written as:

$$\begin{cases} B_x = B_{xr} + B_{xi}i \\ B_y = B_{yr} + B_{yi}i \\ B_z = B_{zr} + B_{zi}i \\ J_x = J_{xr} + J_{xi}i \\ J_y = J_{yr} + J_{yi}i \\ J_z = J_{zr} + J_{zi}i \end{cases} \quad (6)$$

where B_i ($i = x, y, z$) is magnetic flux density component in i direction; B_{xr} and B_{xi} are the real part and imaginary part of the complex quantity B_x , respectively. The same for current density J_i .

When the harmonic electromagnetic field is taken into consideration, the electromagnetic force density changes over time. Hence, the volume force is decomposed into a time-independent component and a time-dependent component. Due to the electromagnetic field period being much shorter than the momentum response time of the liquid steel, the time-averaged Lorentz force should be calculated to investigate the electromagnetic field characteristics [17]. The time-averaged Lorentz force can be calculated as follows:

$$\begin{cases} F_x = \frac{1}{2}Re(J_y \cdot B_z^* - J_z \cdot B_y^*) \\ F_y = \frac{1}{2}Re(J_z \cdot B_x^* - J_x \cdot B_z^*) \\ F_z = \frac{1}{2}Re(J_x \cdot B_y^* - J_y \cdot B_x^*) \end{cases} \quad (7)$$

where, B_i^* is the conjugate complex number of B_i , Re is the real part of the complex quantity F_i . In conclusion, the time-averaged Lorentz force can be written as follow:

$$F_E = \frac{1}{2}Re(\mathbf{J} \times \mathbf{B}^*), \quad (8)$$

Here F_E is the time-averaged Lorentz force, $\text{N} \cdot \text{m}^{-3}$.

2.3. Electromagnetic Torque Model

In addition, the torque produced in the strand is used for evaluating the drive ability of the stirrer to the liquid steel in this study. A new triple integral numerical model is put forward to calculate the electromagnetic torque. The electromagnetic torque that applied to the entire conductor in the harmonic electromagnetic field can be calculated by:

$$T = \iiint_{Vol} (r \times F_E) dVol, \quad (9)$$

where, T is the electromagnetic torque, $\text{N} \cdot \text{m}$; r is the distance from the central axis (Z -axis for this study), m ; Vol is the fixed volume range of the conductor (i.e., probe and strand in this paper) in the computational domain with closed boundary surface.

2.4. Boundary Conditions and Calculating Parameters

1. The excitation source of M-EMS is three-phase alternating current, the phase difference is 120 degree.
2. The magnetic flux parallel boundary condition is applied to the external surfaces of the surrounding air cylinder.
3. An insulating layer is used between the coil and the iron core; another insulating layer is used between the mold and the strand.

The numerical model was carried out by the finite element software Ansys Electromagnetics Suite. The tetrahedral mesh was adopted in the electromagnetic model with about an initial 300 thousand cells, and a mesh adaptive refinement mechanism was conducted after every iteration. Besides, the grids in the copper mold and strand region were more refined to accurately predict the eddy currents. The Dimensions of the model were based on the real stirrer for measurement. The origin of coordinates for the calculation model was at the center of the mold top plane. The positive direction of Z axis was the casting direction. The center plane of the stirrer was located at $Z = 0.54$ m. For saving computation consumption, a 1.40 m long strand from the meniscus was simulated. Tables 1 and 2 demonstrate the main dimensions and the physical properties of materials used in the current study, respectively.

Table 1. Main dimensions of the M-EMS.

Parameter	Value
Sectional dimension [mm^2]	150×150
Mold length [mm]	850
Mold working length [mm]	750
Mold thickness [mm]	12
Outer diameter of stirrer [mm]	880
Inner diameter of stirrer [mm]	544
Height of iron core [mm]	270
Height of stirring coil [mm]	420

Table 2. Physical properties of material employed in this study.

Parameter	Value
Magnetic permeability of vacuum [H m^{-1}]	1.257×10^{-6}
Relative permeability of steel, copper mold, stirring coil and air	1
Relative permeability of iron core	1000
Electrical conductivity of molten steel [S m^{-1}]	7.14×10^5
Conductivity of copper mold (298 K) [18] [S m^{-1}]	4.7×10^7
Conductivity of copper mold (423 K) [18] [S m^{-1}]	3.18×10^7
Conductivity of probe [S m^{-1}]	3.8×10^7

3. Design of the Electromagnetic Torque Measurement Device

In order to measure the electromagnetic torque and verify the accuracy of the numerical model, a well-designed electromagnetic torque measurement device was fabricated in an electrical apparatus plant, an offline mold was used without cooling system. The schematic diagram of the measurement device is shown in Figure 2. The detecting device comprised a measuring system and support unit. The measuring system consisted of a measuring probe, torque transmission rod, torque sensor and display instrument. The support unit was made up of supporting bar and the fixed link, which could be moved up and down.

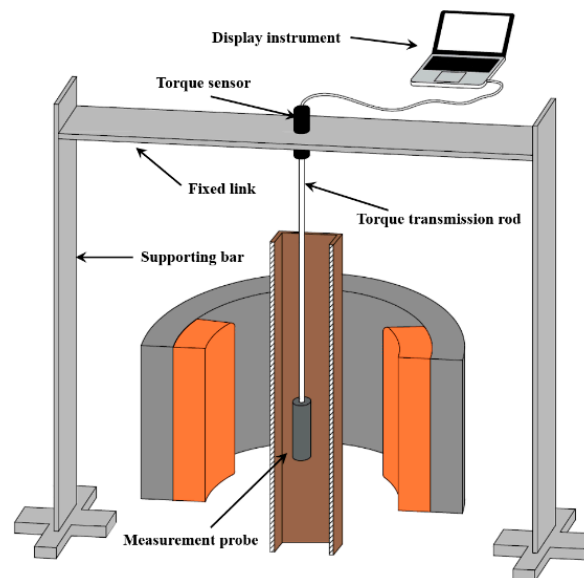


Figure 2. Schematic diagram of the electromagnetic torque measurement device.

Figure 3 reveals the actual electromagnetic torque meter (a) and offline test equipment (b). The model of the torque meter is CEDAR DIS-RL, which contains the sensor part and display part. The electromagnetic torque can not be measured directly without a carrier, so a measuring probe was customized. The probe was made of aluminum due to the distinguishing features in relatively low density and high conductivity properties. The probe was a hollow annulus for portability, fastened to the transmission rod by stainless steel sheets. The outer diameter, inner diameter, and height of the probe were 100 mm, 84 mm and 150 mm, respectively. When the conductive probe was placed into a rotational electromagnetic field in the continuous casting mold with electromagnetic stirring, a rotational motion occurred under the action of electromagnetic torque. The rotation displacement was delivered to the torque sensor by the transmission rod, then translated into an electrical signal. Finally, the value of electromagnetic torque was displayed on the instrument.



Figure 3. Structure photo of the electromagnetic torque measurement device: (a) torque meter; (b) offline test equipment.

4. Model Validation

Figure 4 gives the comparison between the calculated value and measured data of the magnetic flux density: (a) along the centerline of the mold; (b) in the stirrer center under different current

intensity. The measured data of magnetic flux density was obtained through a LakeShore 475DSP gauss meter. The electromagnetic field distribution of the mold was simulated without strand, of which the electrical conductivity of copper mold at the room temperature (approximately 298 K) was employed. It is observed that the calculated value shows good agreement with measured data. In Figure 4b, the predicted magnetic flux density increases linearly with the increase of current intensity. The calculated value is highly consistent with the measured from 0 to 500 A. However, the measured data is a bit lower than the calculated value when the current intensity exceeds 500 A. It seems reasonable because the iron core turns into a magnetically saturated state gradually as the current intensity increases, the conversion efficiency between the electrical and magnetic is decreased, which is not considered in the numerical calculation.

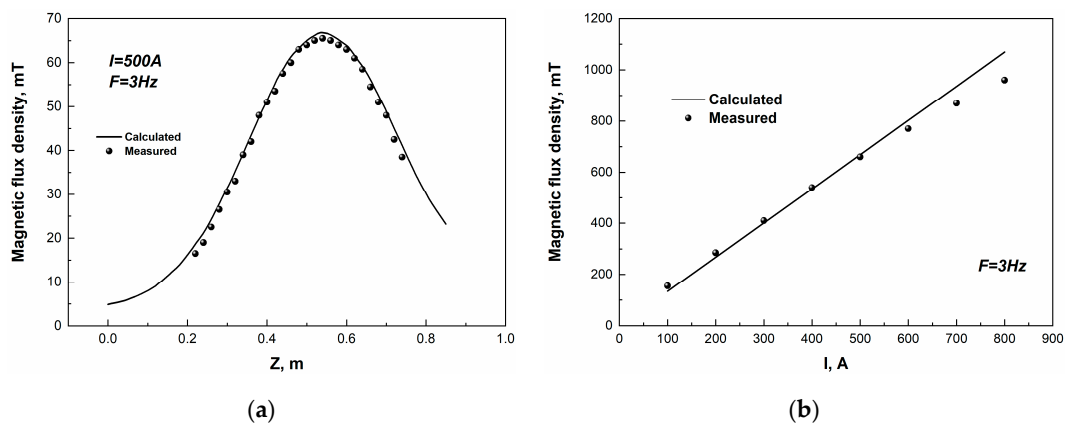


Figure 4. Comparison between calculated and measured data of the magnetic flux density: (a) along the centerline of mold; (b) in the stirrer center.

Figure 5 shows the comparison between the predicted value and measured data of the electromagnetic torque: (a) under different current intensity; (b) under different current frequency. The center of the probe was placed at the stirrer center along the axial direction. As seen in Figure 5a, the measured data is gradually lower than the calculated value with the increase of current intensity, due to the magnetically saturated effect of the iron core. It is seen that the calculated torque and the measured one are basically in coincidence in Figure 5b. However, the measured value is higher than the calculated when the current frequency exceeds 4 Hz. This is because as the measurement time increased, the temperature of the copper tube increased slightly under the effect of joule heat, which reduced the conductivity and the electromagnetic shielding effect of the copper mold. As a result, the measurement value is higher, but the error is within 7%. In summary, the numerical model is reliable.

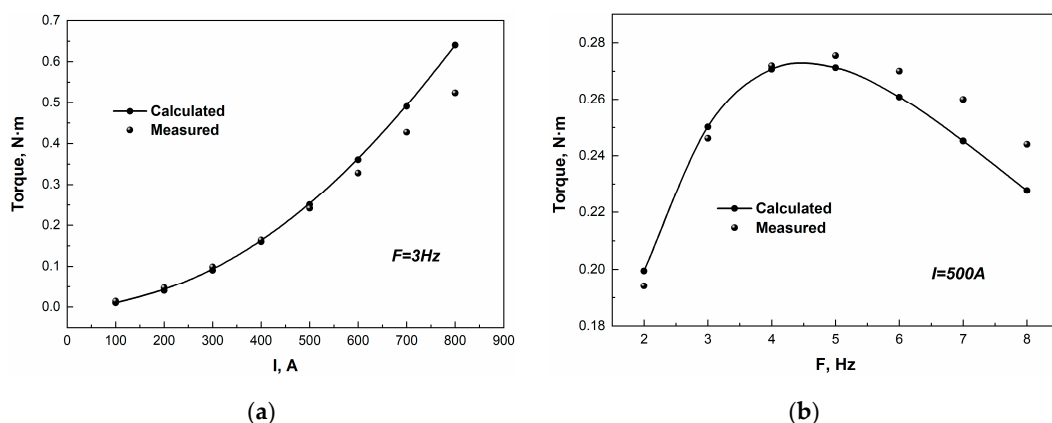


Figure 5. Comparison between predicted and measured data of the electromagnetic torque: (a) under different current intensity; (b) under different current frequency.

5. Results and Discussion

5.1. Electromagnetic Field Characteristics of the Continuous Casting Mold

Figure 6 gives the centerline magnetic flux density distribution under the mold temperatures of 298 and 423 K. It is seen that the magnetic flux density profile is a symmetrical distribution about the center plane of the stirrer, the maximum of the magnetic flux density appears at the center of the stirrer. Besides, the value of the magnetic flux density is larger when the mold actual operation temperature is higher (approximately 423 K). The high temperature of the copper mold leads to a decrease in conductivity, so the electromagnetic shielding effect is reduced. The maximum difference of the magnetic flux density under different mold temperature is 5.68 mT. Therefore, the electrical conductivity of copper mold at 423 K was adopted in the subsequent simulations to meet the real continuous casting condition.

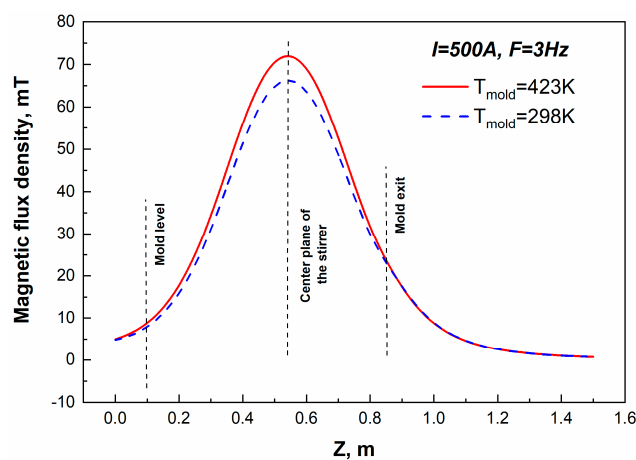


Figure 6. Distribution of magnetic flux density along the strand central axis under the mold temperatures of 298 and 423 K.

Figure 7 displays the contour plot of the time-averaged magnetic flux density on the strand surface. It is seen that according to the casting direction, the magnetic flux density on the strand surface first increased and then decreased. The magnetic flux density was mainly concentrated around the stirrer, and the magnetic flux density on the strand almost disappeared below the mold. Figure 8 presents the vector of the time-averaged electromagnetic force density on the center plane of the stirrer ($Z = 0.54$ m). It is observed that the electromagnetic force rotated anticlockwise on the transverse plane of the strand. It was the largest at four corners, and the closer it was to the center, the smaller it was. Additionally, the electromagnetic force at relative position was equal and opposite, so the electromagnetic torque was generated.

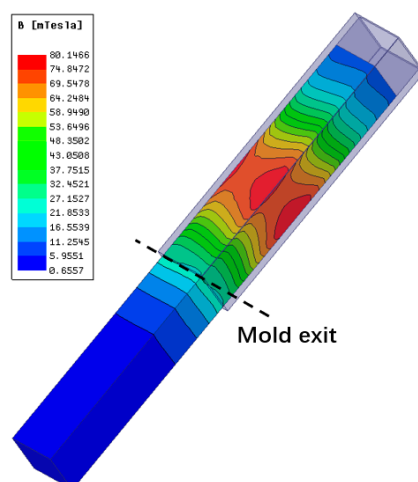


Figure 7. Contour plot of time-averaged magnetic flux density on the strand surface at 500 A/3 Hz.

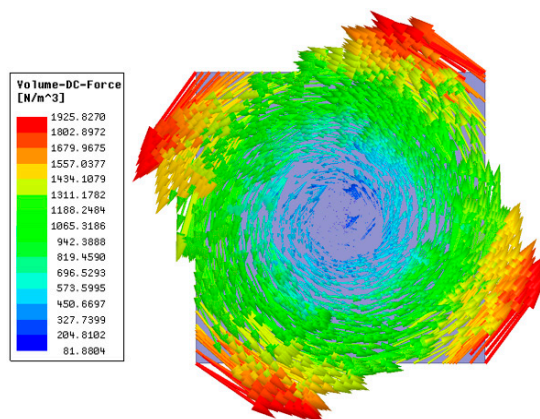


Figure 8. Vector of time-averaged electromagnetic force density on the strand section $Z = 0.54$ m at 500 A/3 Hz.

5.2. Confirmation of the Optimum Frequency

Figure 9 shows the magnetic flux density distribution along the axial direction under different current frequencies. Current frequency has no direct effect on the magnetic flux density according to Ampere's law. However, because of the electromagnetic shielding effect of the copper mold, the magnetic flux density decreased with the increases of current frequency. Outside the mold, the magnetic flux density was the same at all current frequency. The following equation describes the relationship between the stirring intensity F and current frequency [6].

$$F \propto B_M^2(f)f. \quad (10)$$

where, $B_M(f)$ is the magnetic flux density inside the strand, which reduces with the increment of frequency; f is the frequency of excitation source. The force approaches to zero when the frequency is very high because of the small magnetic flux density. Therefore, there is an intermediate value called optimum frequency, at which the stirring intensity is highest. The electromagnetic torque of the strand under different current intensities and frequencies was calculated using the integral model to obtain the optimum frequency, shown in Figure 10. As the current frequency increased, the electromagnetic torque of the strand rose rapidly firstly, then reached the maximum value, and finally decreased gradually. In the present condition, the optimum frequency is 7 Hz. The optimum frequency is increased in comparison with that in Figure 5b due to the adoption of lower mold conductivity. Besides,

the optimum frequencies were all 7 Hz under different current intensities, which indicates that the optimum frequency was not affected by the running current intensity.

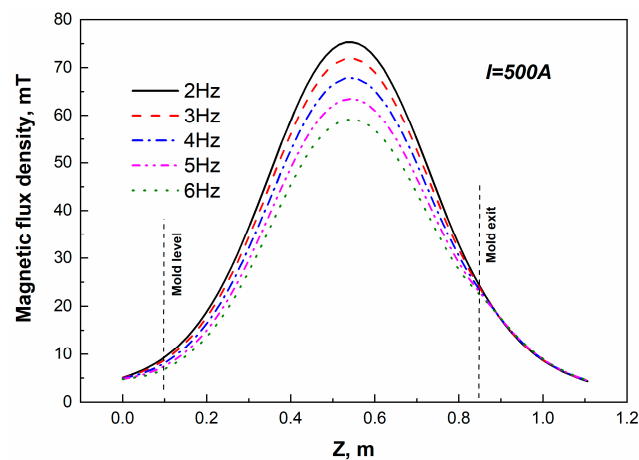


Figure 9. Distribution of centerline magnetic flux density along the axial direction under different current frequencies.

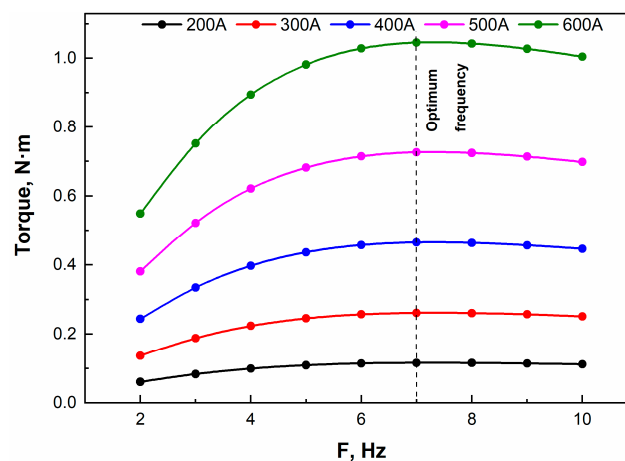


Figure 10. Electromagnetic torque of strand under different current intensities and frequencies.

Considering the penetrability of the electromagnetic field, the optimum frequency is related to the thickness of copper mold and the section size of strand. Five schemes were designed to evaluate the optimal frequency with the same stirrer, which are listed in Table 3. The quantitative calculations are shown in Figure 11. As shown from the figure, the whole electromagnetic torque of the strand was bigger, with a larger section for a specific stirrer under the constant current intensity. Furthermore, the thicker the copper tube and the larger the strand section size, the smaller the optimum frequency. On the other hand, a thinner copper mold could improve the utilization efficiency of the stirrer.

Table 3. Different schemes for evaluating the optimal frequency.

Case	Sectional Dimension [mm ²]	Mold Thickness [mm]
A	150 × 150	12
B	180 × 180	15
C	200 × 200	18
D	220 × 220	20
E	250 × 250	22

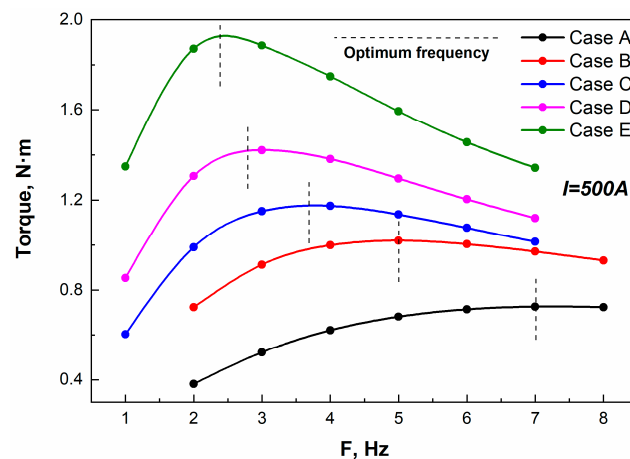


Figure 11. Relationship between the electromagnetic torque of strand and the current frequency under different schemes.

5.3. Effect of Stirring Current Intensity on the Electromagnetic Field

Figure 12 gives the magnetic flux density under different current intensities: (a) along the strand central axis; (b) in the stirrer center. It is seen that the magnetic flux density increased obviously with the increasing current intensity. Because the magnetically saturated effect of the iron core was not considered in the numerical model, there was a favorable linear relationship between the predicted magnetic flux density and the running current. With every 100 A increase in the current intensity, the maximum magnetic flux density increased by 14.40 mT.

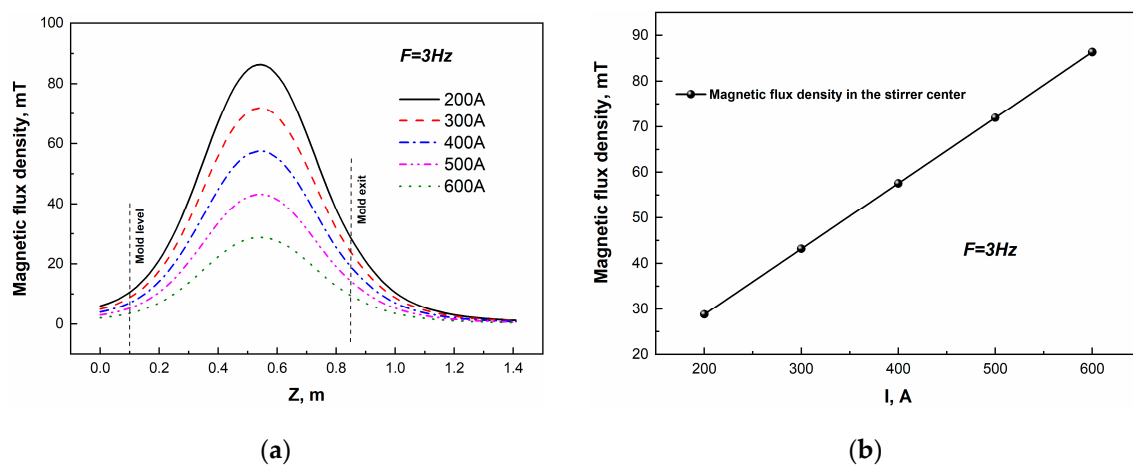


Figure 12. Distribution of magnetic flux density under different current intensities: (a) along the strand central axis; (b) in the stirrer center.

Figure 13a shows the effect of current intensity on the tangential electromagnetic force distribution along the center plane of stirrer. The electromagnetic force significantly increased with the increase in current intensity. The current intensity had great influence on the stirring intensity. The maximal time-averaged electromagnetic force increased from $196 \text{ N}\cdot\text{m}^{-3}$ at 200 A to $1761 \text{ N}\cdot\text{m}^{-3}$ at 600 A. However, the local electromagnetic forces could not accurately reflect the entire strand. The relationship between the electromagnetic torque and the current intensity is shown in Figure 13b. It is seen that the electromagnetic torque of the strand increased distinctly with the increases of current intensity. Besides, the torque is a quadratic function of the stirring current.

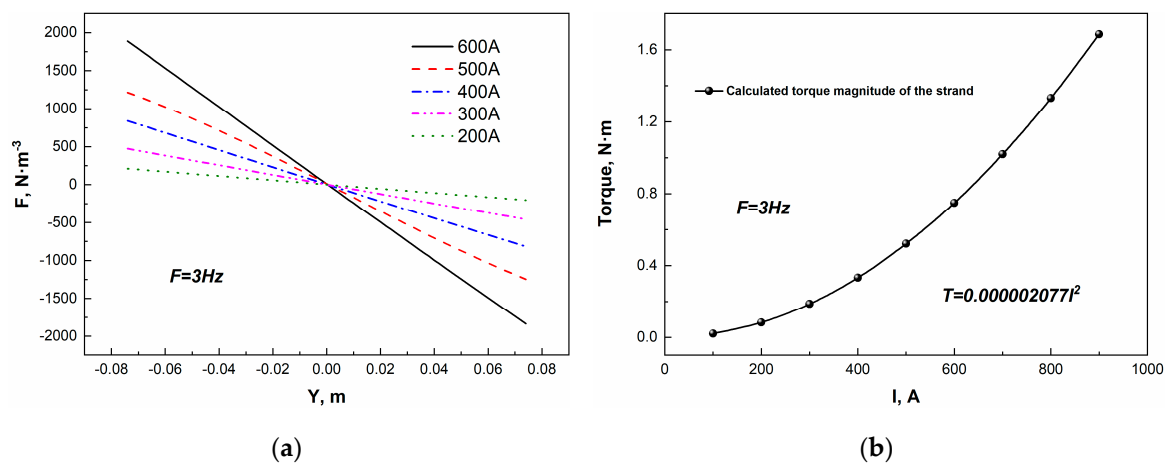


Figure 13. (a) Distribution of time-averaged electromagnetic force along the center plane of the stirrer; (b) Electromagnetic torque of strand under different current intensities.

5.4. Influence of Stirrer Installation Position on the Electromagnetic Field

Table 4 lists the calculation schemes with different installation positions of the stirrer for a $220 \times 220 \text{ mm}^2$ bloom casting with the mold thickness of 20 mm. The Dimensions of the stirrer are consistent with the description in Table 1. Figure 14 presents the contour map of the magnetic flux density on the strand surface under different stirrer installation positions. It can be easily observed that the difference of magnetic flux density distribution is obvious. For case A, the stirrer was in the middle position of mold, the electromagnetic shielding effect of copper mold affected all the electromagnetic field of the strand, and the magnetic flux density at the bottom of mold has almost disappeared. Moreover, a certain magnetic flux density existed in the meniscus region. With the stirrer installed at the lower part of the mold, as in the case B, the magnetic flux density on the strand surface was more widely distributed than in the case A, which maintained about 200 mm below the mold exit. The bottom edge of the stirrer was already below the mold exit position in the case C, the effect of electromagnetic shielding on the magnetic flux density was reduced along the axial direction. The magnetic flux density on the strand surface lasted a distance below the copper mold. Besides, the maximal magnetic flux density appeared at the center of the stirrer for case A and case C. However, the maximal magnetic flux density occurred at the mold exit in the case C. It seems reasonable because that the stirrer center was near the mold exit for case C, and the location of the maximal magnetic flux density moved down under the combined effect of the stirrer installation position and the electromagnetic shielding effect of copper mold.

Table 4. Different schemes for installation position of stirrer.

Case	Distance between the Stirrer Center and Top of the Mold [mm]
A	440
B	590
C	740

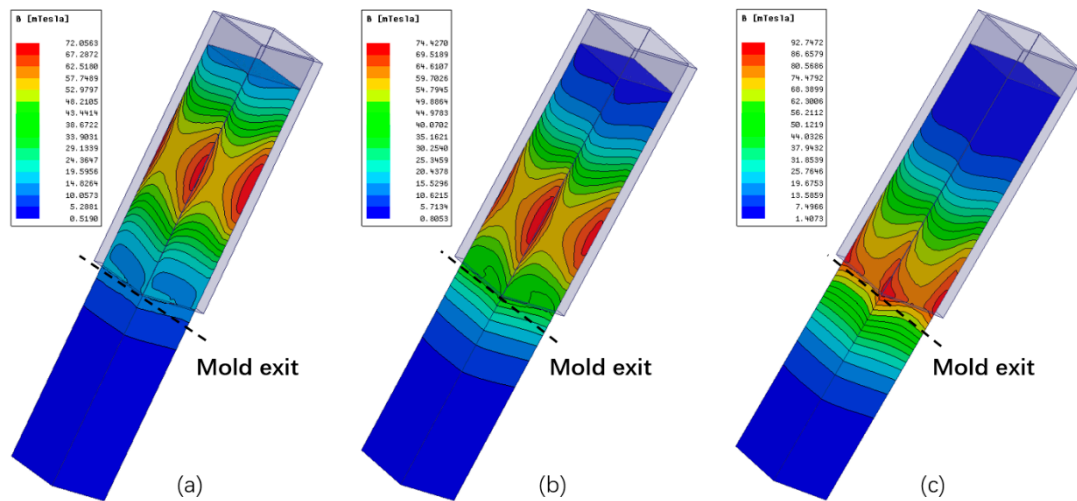


Figure 14. Contour plot of magnetic flux density on the strand surface under different stirrer installation positions at 500 A/3 Hz: (a) Case A; (b) Case B; (c) Case C.

Figure 15a displays the magnetic flux density distribution at the centerline of strand along the casting direction. It is observed that the maximal magnetic flux density on the central axis increased as the installation position of stirrer moved down. The magnetic flux density profile is distributed symmetrically about the center plane of the stirrer for case A and B. However, the axis of symmetry is below the center plane of stirrer in the case C. The electromagnetic torque of strand was compared under different schemes, given in Figure 15b. It is observed that the torque of strand increased clearly with the declining location of the stirrer, the increase in the scheme C is even more obvious. In consequence, the efficiency of stirrer is higher when the stirrer is installed lower. However, on the other hand, if the location of the stirrer is too low, the melt flow in the meniscus zone may be less active for melting the slag, and the electromagnetic stirring may lead to an inhomogeneous initial shell [13].

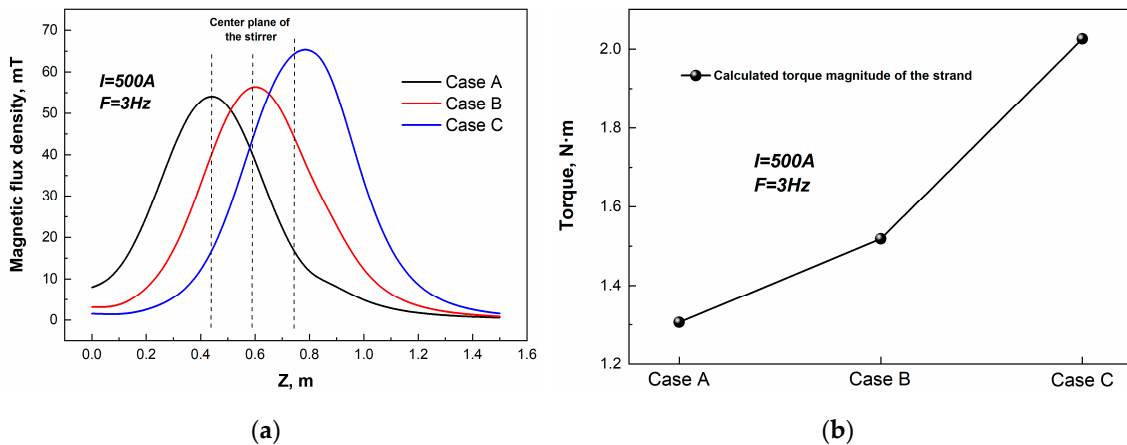


Figure 15. (a) Distribution of magnetic flux density at the centerline of strand along the casting direction; (b) Electromagnetic torque of strand under different stirrer installation positions.

Figure 16 shows the electromagnetic torque of the strand under different current frequencies. It is observed that the strand torque of case A was lower than that of case B under the same current intensity. Furthermore, the optimum frequency of case A was smaller than case B because that the electromagnetic shielding was reduced as the stirrer moved down. For the case C, the electromagnetic torque of strand increased rapidly within 6 Hz and then increased linearly as the frequency rose above 6 Hz. It indicates that the electromagnetic torque increment caused by the increase of frequency was

larger than the weakening caused by the electromagnetic shielding effect of copper mold, which means the optimal frequency no longer exists.

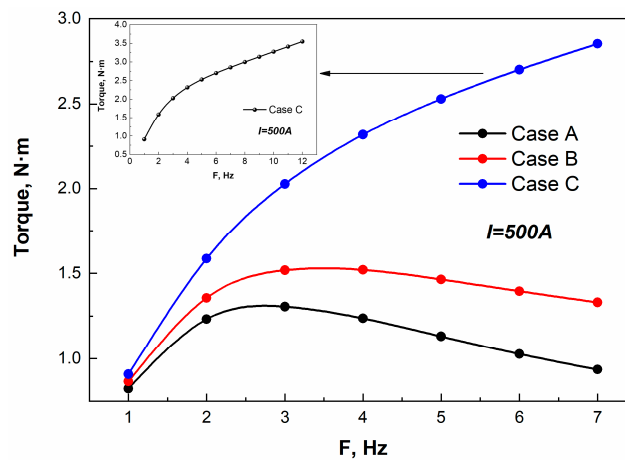


Figure 16. Relationship between the electromagnetic torque of strand and the current frequency under different stirrer installation positions.

6. Conclusions

1. A new integral numerical model is proposed to calculate the electromagnetic torque of the strand, which is used to represent the stirring intensity of a given stirrer. The model is validated using the measured data by an independently designed electromagnetic torque measurement device.
2. With regard to the specific mold with electromagnetic stirring, an optimum frequency existed to maximize the stirring intensity. The optimum frequency can be confirmed by the maximal value of the strand electromagnetic torque. Furthermore, the thicker the copper mold and the larger the strand section size, the smaller the optimum frequency.
3. The magnetic flux density increases linearly with the increases of current intensity. The electromagnetic force increases remarkably as the current intensity increases, and the electromagnetic torque of the strand is a quadratic function of the running current.
4. The installation position of the stirrer has great influence on the electromagnetic field distribution because of the electromagnetic shielding effect of copper mold. The optimum frequency is bigger and the efficiency of stirrer is higher when the stirrer is installed lower. Besides, the law of the optimal frequency changes if the installation position of the stirrer is too much lower than the mold exit.

Author Contributions: Conceptualization, S.L. and J.Z.; methodology, S.L.; software, S.L.; validation, S.L., P.W. and H.X.; investigation, S.L.; resources, S.L., H.X. and J.Z.; writing—original draft preparation, S.L.; writing—review and editing, S.L. and J.Z.; visualization, S.L. and H.L.; supervision, J.Z.

Funding: This research was funded by the National Natural Science Foundation of China (Grant Number U1860111).

Acknowledgments: We are grateful to Jin Li from SteelFlow ElectroMagnetic Corporation Ltd. and Zhen Lu from Sinosteel Corporation for their help in technical support.

Conflicts of Interest: The authors declare no conflict of interest.

References

1. Sun, H.; Zhang, J. Macro-segregation improvement by swirling flow nozzle for bloom continuous castings. *Metall. Mater. Trans. B* **2014**, *45*, 936–946. [[CrossRef](#)]
2. Li, S.; Lan, P.; Tang, H.; Tie, Z.; Zhang, J. Study on the Electromagnetic Field, Fluid Flow, and Solidification in a Bloom Continuous Casting Mold by Numerical Simulation. *Steel Res. Int.* **2018**, *89*, 1800071. [[CrossRef](#)]

3. AYATA, K.; MORI, T.; FUJIMOTO, T.; OHNISHI, T.; WAKASUGI, I. Improvement of macrosegregation in continuously cast bloom and billet by electromagnetic stirring. *Trans. Iron Steel Inst. Jpn.* **1984**, *24*, 931–939. [[CrossRef](#)]
4. Shin, Y.K.; Lee, I.R.; Kim, D.S.; Kim, S.K.; Oh, K.S. Construction and Start-up of a Billet Caster at Pohang Works. *Ironmak. Steelmak.* **1988**, *15*, 143–149.
5. Kitamura, M.; Kojima, S.; Onishi, T.; Kawasaki, S. Production of High-Grade Wire Rod from Large-Section Continuously Cast Bloom. *Ironmak. Steelmak.* **1983**, *10*, 82–90.
6. Sahoo, P.P.; Kumar, A.; Halder, J.; Raj, M. Optimisation of electromagnetic stirring in steel billet caster by using image processing technique for improvement in billet quality. *ISIJ Int.* **2009**, *49*, 521–528. [[CrossRef](#)]
7. Kunstreich, S. Electromagnetic stirring for continuous casting. *Rev. Métallurgie-Int. J. Metall.* **2003**, *100*, 395–408. [[CrossRef](#)]
8. Kunstreich, S. Electromagnetic stirring for continuous casting-Part 2. *Rev. Métallurgie-Int. J. Metall.* **2003**, *100*, 1043–1061. [[CrossRef](#)]
9. An, H.; Bao, Y.; Wang, M.; Yang, Q. Electromagnetic torque detecting for optimization of in-mould electromagnetic stirring in the billet and bloom continuous casting. *Ironmak. Steelmak.* **2018**, 1–10. [[CrossRef](#)]
10. Beitelman, L. Effect of mold EMS design on billet casting productivity and product quality. *Can Metall. Q.* **1999**, *38*, 301–309. [[CrossRef](#)]
11. Yang, Z.G.; Wang, B.; Zhang, X.F.; Wang, Y.T.; Dong, H.B.; Liu, Q. Effect of electromagnetic stirring on molten steel flow and solidification in bloom mold. *Iron Steel Res. Int.* **2014**, *21*, 1095–1103. [[CrossRef](#)]
12. Wang, X.; Wang, S.; Zhang, L.; Sridhar, S.; Conejo, A.; Liu, X. Analysis on the deflection angle of columnar dendrites of continuous casting steel billets under the influence of mold electromagnetic stirring. *Metall. Mater. Trans. A* **2016**, *47*, 5496–5509. [[CrossRef](#)]
13. Li, S.; Lan, P.; Zhang, J. Numerical Simulation of Turbulence Flow and Solidification in a Bloom Continuous Casting Mould with Electromagnetic Stirring. In *TMS Annual Meeting & Exhibition, the International Symposium on CFD Modeling and Simulation in Materials Processing*; Springer: Cham, Switzerland, 2018; pp. 223–236.
14. Trindade, L.B.; Nadalon, J.E.A.; Contini, A.C.; Barroso, R.C. Modeling of solidification in continuous casting round billet with mold electromagnetic stirring (M-EMS). *Steel Res. Int.* **2017**, *88*, 1600319. [[CrossRef](#)]
15. Davidson, P.A.; Hunt, J.C.R. Swirling recirculating flow in a liquid-metal column generated by a rotating magnetic field. *J. Fluid Mech.* **1987**, *185*, 67–106. [[CrossRef](#)]
16. Davidson, P.A. Magneto-hydrodynamics in materials processing. *Annu. Rev. Fluid Mech.* **1999**, *31*, 273–300. [[CrossRef](#)]
17. Zhang, H.; Nagaumi, H.; Zuo, Y.; Cui, J. Coupled modeling of electromagnetic field, fluid flow, heat transfer and solidification during low frequency electromagnetic casting of 7XXX aluminum alloys: Part 1: Development of a mathematical model and comparison with experimental results. *Mater. Sci. Eng. A* **2007**, *448*, 189–203. [[CrossRef](#)]
18. Trindade, L.B.; Vilela, A.C.; Vilhena, M.T.; Soares, R.B. Numerical model of electromagnetic stirring for continuous casting billets. *IEEE Trans. Magn.* **2002**, *38*, 3658–3660. [[CrossRef](#)]

